Gravity compensation of a 2R1T mechanism with remote center of motion for minimally invasive transnasal surgery applications

Ataol Behram Aldanmaz, Orhan Ayit⬡, Gökhan Kiper*⬡ and Mehmet İsmet Can Dede⬡

Department of Mechanical Engineering, Izmir Institute of Technology, 35430 Izmir, Turkey
*Corresponding author. E-mail: gokhankiper@iyte.edu.tr

Abstract

This work addresses the gravity balancing of a 2R1T (2 rotations – 1 translation) mechanism with remote center of motion. A previously developed balancing solution is modified and applied to a prototype, and test results are presented. The mechanism is an endoscope holder for minimally invasive transnasal pituitary gland surgery. In this surgery, the endoscope is inserted through a nostril of the patient through a natural path to the pituitary gland. During the surgery, it is vital for the manipulator to be statically balanced so that in case of a motor failure, the patient is protected against any harmful motion of the endoscope. Additionally, static balancing takes the gravitational load from the actuators and hence facilitates the control of the mechanism. The mechanism is a 2URRR-URR type parallel manipulator with three legs. The payload mass is distributed to the legs on the sides. By using counter-masses for two links of each leg, the center of mass of each leg is lumped on the proximal link which simplifies the problem of balancing of a two degree-of-freedom inverted pendulum. The two proximal links with the lumped mass are statically balanced via springs. Dynamic simulations indicate that when the mechanism is statically balanced, generated actuator torques are reduced by 93.5%. Finally, the balancing solution is implemented on the prototype of the manipulator. The tests indicate that the manipulator is statically balanced within its task space when the actuators are disconnected. When the actuators are connected, the torque requirements decrease by about 37.8% with balancing.

1. Introduction

A mechanism is statically balanced when its total potential energy is kept constant in any configuration of the mechanism. For a mechanism in static equilibrium, the actuators do not work to sustain any conservative force acting on its moving members [1].

In most applications, assuming perfect rigidity of the mechanical members, the change in the potential energy of a mechanism is due to gravitational effects, and in this case, static balancing corresponds to gravity balancing or gravity compensation. There are several ways to obtain gravity balancing for parallel manipulators. If the overall center of mass (CoM) of the mechanism could be kept at the same level of height for any given configuration, the static balance is obtained. This is important because the unbalanced forces could cause adverse effects in the operation of the mechanism such as vibrations and joint wear [2]. Another way to obtain a statically balanced mechanism is to keep its total energy constant so it could be statically balanced in the direction of the gravity vector [3].

A statically balanced system has many advantages over an unbalanced system. Statically balanced systems have a very good energy exchange between the energy storage elements and the system; therefore, the mechanism needs minimal external energy input for operation. The decrement in the operating effort of the actuators gives opportunity for usage of smaller actuators since the actuators no longer

work for compensating the gravitational effects. For a statically balanced system, the external energy input would be needed to cover the energy losses due to friction and to accelerate the mechanism [4].

The types of static balancers that are issued in this work are the counter-masses and springs. The main idea of using counter-mass is to exchange the gravity potential between the counter-mass and the balanced mass. One of the disadvantages of this balancing method is that it increases the inertia of the system, and the added masses could collide with the links within the workspace. In spring balancers, the change in gravitational potential energy in the system is compensated with springs. It is relatively easy to balance a mass which rotates about a fixed axis, but usually additional links are required for balancing floating links. This study makes use of both counter-masses and springs for gravity compensation.

Many researchers have worked on static balancing of parallel and serial manipulators for planar and spatial motion. For example, [5] worked on an algorithm for balancing serial and parallel mechanisms where counter-masses, springs, and combination of counter-masses and springs are used together. Wang and Kong [6] developed a geometric method for static balancing of spherical mechanisms. Van Dorsser et al. [7] developed a system to adjust a spring and a linkage-based balancer by changing the active coils of the spring which effects its spring stiffness and allows the system to stay in balance when the payload changes in an energy-conserving way. Yaşir et al. [8] and Maaroof et al. [9] have introduced two different partial gravity compensation solutions with springs for a 2URRR-URR parallel manipulator. Maaroof et al. [9] achieved partial gravity compensation by using torsional springs on actuator shafts.

The 2URRR-URR parallel manipulator is designed as an endoscope holder for minimally invasive transnasal pituitary gland surgery application by ref. [10]. In this work, the balancing solution of ref. [8] is slightly modified and formulated in detail. The balancing solution is implemented in parallel with the constructional design of the balancing components. The solution is verified via simulations and tested on the manipulator's prototype. The presented methodology can be used for gravity balancing of parallel manipulators.

2. Description of the system and the need of static balancing

In the surgical system, called NeuRoboScope, the endoscope holder is a parallel manipulator assembled on a passive serial arm (Fig. 1(a)) which can be manually positioned by the surgeon during the surgery [11]. The end-effector of the parallel manipulator which holds the endoscope is placed through the nostril of the patient where there is a natural path to the pituitary gland. The surgeon uses additional surgical tools manually to remove the tumor. The endoscope is pivoted at the upper portion of a nostril, and it should be oriented (pitch and yaw motions) about and move along the pivot point (heave motion) (Fig. 1(b)). Without any static balancing, the torques generated by the motors during the operation are relatively high. Consequently, without the static balancing, the system is harder to control, it consumes more energy, and also in case of a malfunction, the manipulator is not able to keep the position of the endoscope and may cause serious damage to the patient.

The parallel manipulator has 3 degree-of-freedoms for the 2 R1T (2 rotations – 1 translation) motion required for orienting and the heave motion of the endoscope about the pivoting point, which is a remote center of motion (RCM) for the mechanism. The RCM mechanism has a 2URRR-URR kinematic structure, where U and R stand for universal and revolute joints, respectively (Fig. 2). The moving platform is connected to the base of the manipulator with three legs. Each leg comprises a proximal link which is connected to the base with a U joint, a middle link which is connected to the proximal link with an R joint, and a distal link which is connected to the middle link with an R joint. The moving platform is rigidly attached to the distal link of the middle leg, whereas the distal links of the two side legs can rotate with respect to the moving platform about the endoscope axis via circular sliders. Therefore, the side legs have a URRR structure, whereas the middle leg has a URR structure.

The legs define 3 planes intersecting along the endoscope axis. The 3 leg planes can rotate about 3 fixed axes on the base, which intersect at the RCM. The rotary actuators on the side legs have fixed axes on the base and actuate the first R axes of the U joints. The side leg actuators change the angle of
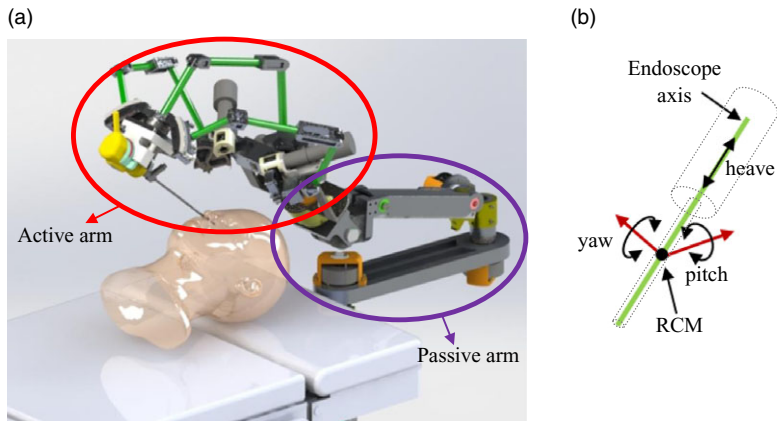
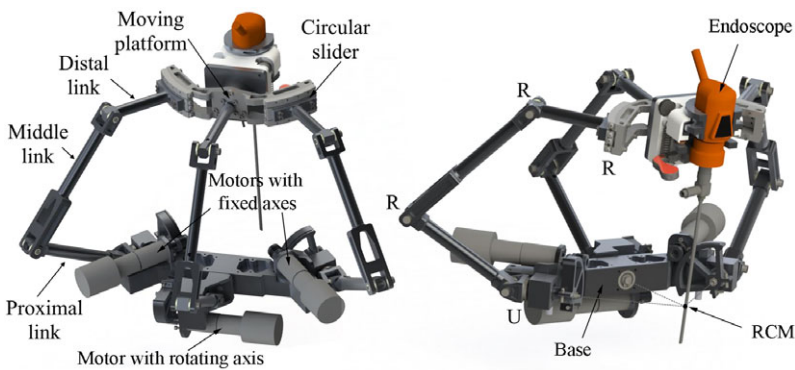**Figure 1.** *(a) NeuRoboScope system [11] and (b) Endoscope motions.*

Figure 2. *The components of the 2URRR-URR parallel manipulator [10].*

the side leg planes with respect to the base plane, hence changing the intersection line of the plane. So side leg actuators are responsible for the orientation of the endoscope. The actuator on the middle leg actuates the second axis of the U joint, which is an axis perpendicular to the middle leg plane and can rotate about the first axis of the U joint. The middle leg actuator moves the endoscope like the slider of a slider-crank linkage on the middle leg plane; hence, it is responsible for the heave motion of the endoscope. The kinematic model and design of the mechanism are presented by ref. [10].

A prototype of the NeuRoboScope system is built and presented by ref. [11]. The requirements of the balancing system to be implemented for this surgical system are as follows: (1) the passive robotic arm end-effector has 13 kg load limit, so the balanced system should have less than 13 kg mass and it is safer to have limited increase in the total inertia of the system, and (2) the additional parts for static balancing should not cause any link collisions. In order to avoid link collisions, the middle leg is not used for static balancing and the payload mass is distributed to two of the legs on the sides.

According to the abovementioned requirements, using counter-masses, CoM of each leg on the sides is lumped to the proximal link attached to the base platform. Hence, the balancing problem is simplified to a basic gravity equilibrator [4], that is, a spring-balancer for an inverted pendulum.

3. Implementation of the static balancing methods on the surgical robot

The counter-mass and spring balancing solution proposed by ref. [8] for a leg is depicted in Fig. 3. The mass of the moving platform including the endoscope is equally distributed to the side legs, and this
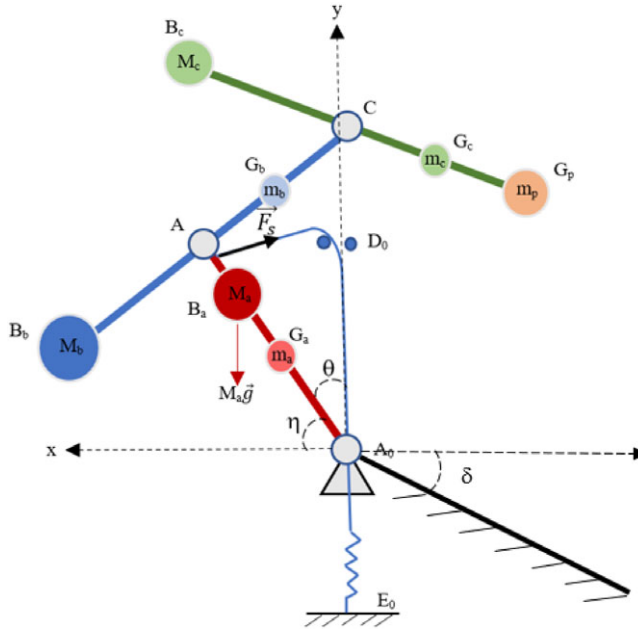
Figure 3. *Diagram for static balancing of a leg with two counter masses and a spring.*

half mass is denoted by m_p. The mass of the distal link is m_c with CoM at G_c, mass of middle link is m_b with CoM at G_b, and mass of proximal link is m_a with CoM at G_a. The counter-mass M_c at B_c is used to balance m_p and m_c, to relocate the total CoM of the distal link to joint C. The counter-mass M_b at B_b is used to balance the total masses of the distal and middle links, to relocate the total CoM of the two links to joint A. Together with the mass m_a of the proximal link with CoM at G_a, the total CoM of the whole leg is at B_a with mass M_a.

Following similar steps, an equivalent inverted pendulum can be obtained for any articulated kinematic chain with revolute, universal, or spherical joints. For the inverted pendulum with rotation center A_0, the rotational degree of freedom of the joint at A_0 may be 1, 2, or 3, and the pendulum can be balanced with a spring [4].

The link lengths and the mass locations are represented as $r_c = |CG_p|$, $r_b = |AC|$, $r_a = |AA_0|$, $b_c = |CB_c|$, $b_b = |AB_b|$, $g_c = |CG_c|$, $g_b = |AG_b|$, $g_a = |A_0G_a|$ and $g_{a,t} = |A_0B_a|$. The payload location is assumed to be at $g_{pay} = |CG_p| = r_c$. The gravity acts along $-y$ direction in Fig. 3, and η is the angle between the proximal link and the x-axis. According to the design by ref. [10], $\eta_{max} = 89.63°$ and $\eta_{min} = -64.11°$. The base plane of the manipulator makes an approximate angle $\delta = 28.5°$ with the horizontal. This is an average value for the manipulator orientation, and the balancing is partial when δ takes some other value when locating the manipulator using the passive arm.

Using a basic gravity equilibrator, one end of the balancing spring is fixed at an arbitrary point on the base (point E_0 in Fig. 3), whereas a thin wire is attached to the other end. The thin wire passes through point D_0, which should be located on a vertical line passing through A_0, the center of the universal joint. The other end of the wire is connected to the proximal link. The length of the wire is adjusted so that the spring is unloaded when the proximal link is at an upright position, that is, along A_0D_0. By this way, a system which behaves as a zero-length spring is obtained [4].

The workspace of the manipulator was defined by ref. [12] from the data of a computed tomography scan. With the results modified after considering the safety conditions and the results changing from patient to patient, the workspace of the manipulator is selected as $\Delta\psi = 40°$ for the yaw motion, $\Delta\phi = 30°$ for the pitch motion, and $\Delta d = 100$ mm for the heave motion of the endoscope. According to
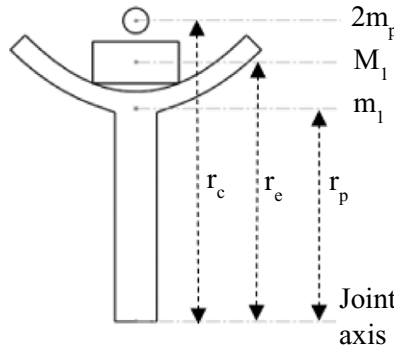
Figure 4. *Payload mass calculation.*

the selected workspace, link lengths of each leg are $r_c = |CG_p| = 200$ mm, $r_b = |AC| = 195$ mm and $r_a = |AA_0| = 135$ mm [10].

The formulations for the counter mass values and locations and spring design are described below. First, the equivalent payload mass is calculated. In Fig. 4, $2m_p$ is the equivalent payload mass, M_1 is the endoscope group mass, and m_1 is the middle leg distal link mass which includes the moving platform that carries the endoscope.

The payload mass $2m_p$ is to be located at a distance $r_c = |CG_p| = 200$ mm from the axis of the R joint between the distal link and the proximal link. So,

$$2m_p r_c = M_1 r_e + m_1 r_p \Rightarrow m_p = \frac{M_1 r_e + m_1 r_p}{2r_c} \tag{1}$$

For selected locations of the counter-masses, the counter-mass values can be computed from (see Fig. 3):

$$M_c b_c = m_c g_c + m_{pay} r_c \Rightarrow M_c = \frac{m_c g_c + m_{pay} r_c}{b_c} \tag{2}$$

$$M_b b_b = m_b g_b + \left(M_c + m_c + m_{pay}\right) r_b \Rightarrow M_b = \frac{m_b g_b \left(M_c + m_c + m_{pay}\right) r_b}{b_b} \tag{3}$$

The total leg mass, M_a, and the location of the CoM of the whole leg, $g_{a,t}$:

$$M_a = m_c + m_{pay} + m_b + m_a + M_c + M_b \tag{4}$$

$$M_a g_{a,t} = M_a r_a + m_a g_a \Rightarrow g_{a,t} = \frac{M_a r_a + m_a g_a}{M_a} \tag{5}$$

When all masses are lumped to point B_a, the problem of balancing has been reduced to a basic gravity equilibrator problem [4] as shown in Fig. 5.

Let $e = |A_0 C_a|$, $f = |A_0 D_0|$ and $s = |D_0 C_a|$. The spring force F_s is proportional to length $|D_0 C_a|$:

$$F_s = ks \tag{6}$$

where k is the spring constant. By using sine theorem in triangle $A_0 C_a D_0$

$$\frac{f}{\sin \alpha} = \frac{s}{\sin \theta} \Rightarrow s = \frac{f \sin \theta}{\sin \alpha} \tag{7}$$

Then by using Eqs. (6) and (7) and moment equilibrium for M_a about A_0, spring coefficient is determined as:

$$g_{a,t} M_a g \sin \theta = e F_s \sin \alpha = eks \sin \alpha = efk \sin \theta \Rightarrow k = \frac{g_{a,t} M_a g}{ef} \tag{8}$$
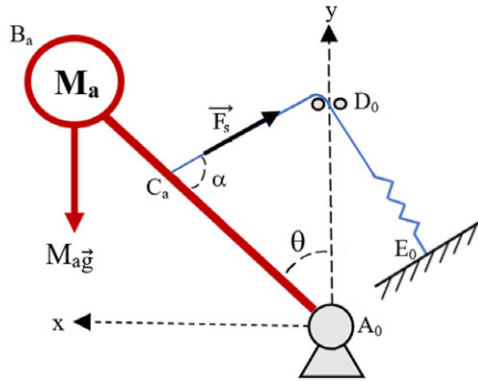
where g is the gravitational acceleration.

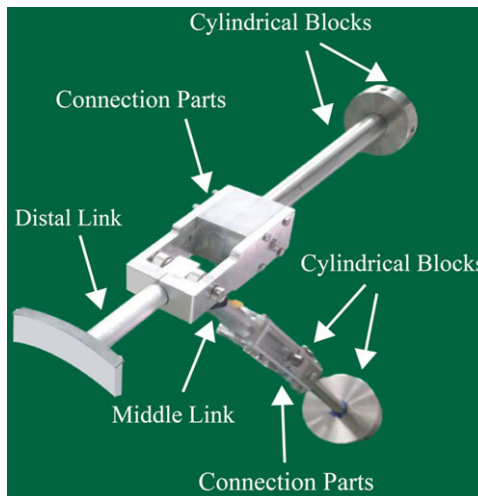**Figure 5.** *Diagram for a basic gravity equilibrator.*

Figure 6. *Counter-mass constructional design for middle and distal links.*

The mass values M_1, m_1, m_c, m_b, and m_a are measured from the parts of the available prototype. The CoM locations (g_c, g_b, g_a) are determined using CAD models. Following Eqs. (1)–(8), the parameters to be selected are b_c and b_b for the counter-mass locations and e and f for the spring constant and wire connection locations. The constructional design details also should be taken into account when determining b_c and b_b. Each counter-mass is designed to have two main parts. One of the parts is an adjustable mass, and the other is to connect this additional mass to the corresponding link (Fig. 6). The connection parts have a constant mass and CoM position with respect to their corresponding joint axes. Cylindrical blocks are selected as the adjustable masses because of the ease of changing their dimensions.

The distal link counter-mass consists of four parts named *D_CM_P1*, *D_CM_P2*, *D_CM_P3,* and *D_CM_P4*. The parts *D_CM_P1* and *D_CM_P2* are parts of the connection elements and *D_CM_P3* and *D_CM_P4* are the cylindrical blocks. The unknowns to be determined are the height and radius of the cylindrical blocks.

In Fig. 7, the total mass of the connection parts is denoted with m_1 positioned at distance a with respect to the joint axis, and the total mass of the cylindrical blocks is denoted with m_2 positioned at distance c with respect to the joint axis. The radius and height for *D_CM_P3* (thin and long cylinder) are r_d and h_1, respectively, and the radius and height for *D_CM_P4* are r_e and h_2, respectively. Due to the
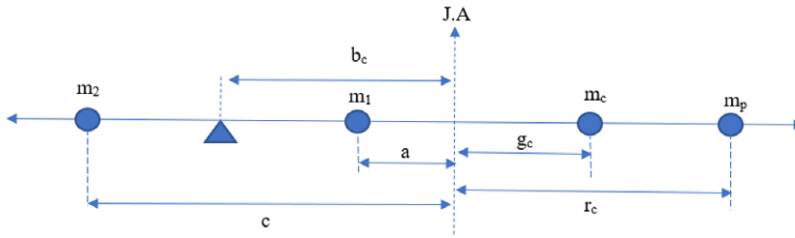
Figure 7. *Distal link counter mass components mass calculations with respect to moment equilibrium.*
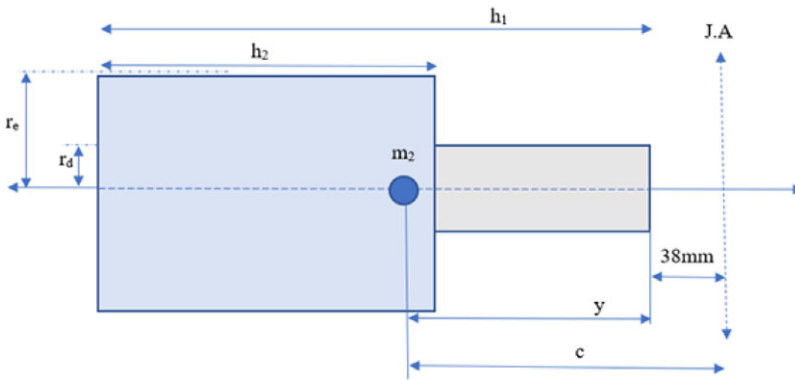

Figure 8. *Balancing cylinders.*

constructional design considerations, *D_CM_P3* is placed through the connection element *D_CM_P2,* and therefore, r_d dimension is set. When *D_CM_P3* is mounted on *D_CM_P2*, the base of the cylinder *D_CM_P3* has a fixed distance of 38 mm with respect to the joint axis as shown in Fig. 8. To calculate the remaining unknowns, moment equilibrium equations are written with respect to the joint axis. The density for parts *D_CM_P3* and *D_CM_P4* are denoted with d_1 and d_2, respectively.

h_2 can be determined in terms of h_1 as follows:

$$d_1 \pi r_d^2 h_1 + d_2 \pi h_2 \left(r_e^2 - r_d^2 \right) = \frac{m_c g_c + m_p r_c}{b_c} - m_1 \Rightarrow h_2 = \frac{A - B h_1}{E} \tag{9}$$

where $A = \dfrac{m_c g_c + m_p r_c}{b_c} - m_1$, $B = d_1 \pi r_d^2$ and $EC = d_2 \pi \left(r_e^2 - r_d^2 \right)$.

To find h_1, a moment equilibrium for the masses located on the distal link is written with respect to the joint axis:

$$-\frac{E}{2} h_2^2 + E \left(h_1 + 38 \right) h_2 + \frac{B}{2} h_1^2 + 38 B h_1 = m_c g_c + m_p r_c - m_1 a \tag{10}$$

Substituting Eq. (9) in Eq. (10), a second-order polynomial in terms of h_1 is found and solved as:

$$M h_1^2 + N h_1 + Q = 0 \Rightarrow h_1 = \frac{-N \pm \sqrt{N^2 - 4MQ}}{-2M} \tag{11}$$

where $M = \dfrac{B^2}{E} + \dfrac{B}{2}$, $N = -\dfrac{AB}{E} - A$ and $Q = \dfrac{A^2}{2E} - 38A + m_c g_c + m_p r_c - m_1 a$. To compute h_1 and h_2, r_e should be specified. Once h_1 is found, h_2 can be calculated from Eq. (9).

The counter-mass for the middle link consists of five parts for the connection and adjustable counter-mass. Same as the distal link's counter-mass, the adjustable masses are cylindrical blocks. The cylindrical blocks are named as *CM_P3* and *CM_P4*. Height and radius of *CM_P3* are denoted with
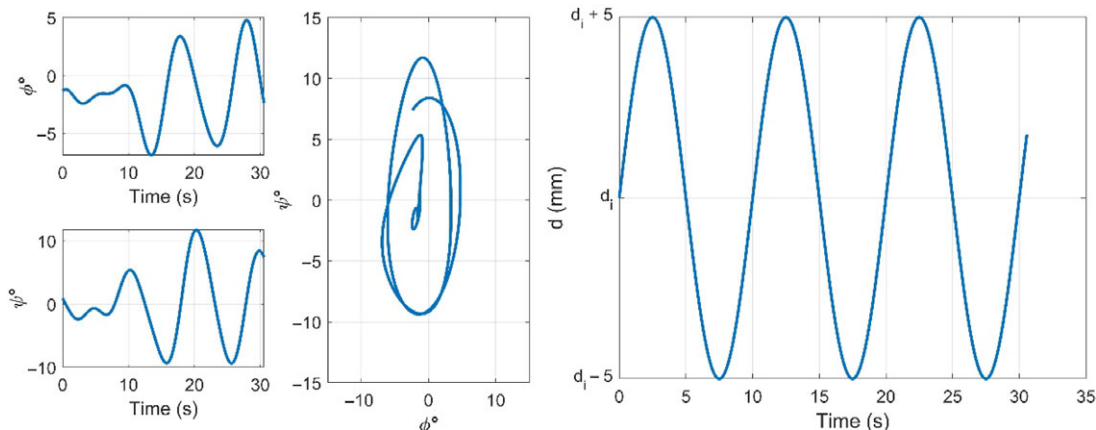
Figure 9. *Trajectory of the pitch (φ) and yaw (ψ) angles and displacement d.*

h_3 and r_f and for *CM_P4* h_4 and r_g, respectively. The unknowns (h_4, h_3, and r_g) are calculated with the same method used in distal link counter-mass calculations.

There are several design considerations to determine the counter-mass distances b_b and b_c. They cannot be set unlimited, because after some point they may collide with the surroundings and block the sight of the surgeon since the manipulator is positioned in between the surgeon and the monitor of the endoscope. On the other hand, it is better to have them as long as possible to decrease total mass of the system. Also, although the balancing eliminates the gravitational effects, the inertia is increased and the motor has to compensate for the inertial force and moments due to the additional masses. In order to see the effect of b_b and b_c, a dynamical model of the system is constructed using MATLAB Simulink. The model of the robot is directly transferred from the CAD model to MATLAB via Multibody blocks. The trajectory of the end-effector used in simulations was obtained from workspace studies conducted by ref. [13], and the trajectory was measured by asking a surgeon to move the endoscope around the nostril of a cadaver. The trajectories for pitch (φ) and yaw (ψ) angles are shown in Fig. 9 where the frequency of motion is approximately calculated as 0.1 Hz. By using this information and workspace studies, the trajectory for translation motion is designed where d_i refers to initial of position d and d_i is chosen at 155, 200, and 245 mm in simulations.

The simulation is run for 50 mm $\leq b_b \leq 300$ and 100 mm $\leq b_c \leq 300$ mm for 5 mm increments of b_b and b_c. The following set of conditions are set for r_e, h_1 and h_2: (1) height of $D\_CM\_P2 + h_2 < h_1 \leq 270$ mm and (2) $r_e/2 < h_2 \leq 80$ mm for both middle and distal links.

To compare the torque values for each combination of b_b and b_c, the average of the calculated root-mean-square (RMS) torque values is calculated by Eq. (12):

$$G_{RMS} = \sqrt{\frac{(RMS\_1)^2 + (RMS\_2)^2 + (RMS\_3)^2}{3}} \tag{12}$$

where *RMS_1*, *RMS_2*, and *RMS_3* are the RMS torque values for the left, right, and middle leg actuators, respectively. By changing r_g and r_e values, the most compact design with the smallest total mass value is calculated using MATLAB. The resulting parameters are tabulated in Table I.

It is seen from the simulation results that without balancing components on the manipulator, $G_{RMS} = 3.06$ N·m for the static analysis (no inertial effects) and $G_{RMS} = 3.08$ N·m for the dynamic analysis. It is seen that gravitational effects outweigh dynamic effects. When the balancing components are included according to the dimensions given in Table I, the G_{RMS} value in the dynamic analysis has decreased to 0.2 N·m which is a 93.5% decrease. The minimum torque values are obtained where d is at its maximum value of 250 mm which is the position where the tip of the endoscope is positioned at the

Table I. *Calculated design parameters of balancing components.*

| LEFT LEG	m_c (gr) 111.3	g_c (mm) 75.90938	h_1 (mm) 192.4055	b_c (mm) 115	M_c (gr) 843.5869	k (N/mm) 1.8041
	m_b (gr) 115.8	g_b (mm) 118.2294	h_2 (mm) 12.09209	b_b (mm) 220	M_b (gr) 1301.107	f (mm) 80.22409
	m_a (gr) 73.3	g_a (mm) 75.66227	h_3 (mm) 244.0932	$g_{a,t}$ (mm) 133.4939	M_a (gr) 2887.913	e_L (mm) 26.13059
	m_p (gr) 442.8189	g_p (mm) 200	h_4 (mm) 29.70822			
RIGHT LEG	m_c (gr) 112.1	g_c (mm) 75.92179	h_1 (mm) 192.64	b_c (mm) 115	M_c (gr) 844.1271	k (N/mm) 1.5919
	m_b (gr) 116.1	g_b (mm) 118.2503	h_2 (mm) 12.06032	b_b (mm) 220	M_b (gr) 1302.467	f (mm) 80.22409
	m_a (gr) 74.4	g_a (mm) 77.68955	h_3 (mm) 244.0003	$g_{a,t}$ (mm) 133.5256	M_a (gr) 2892.013	e_R (mm) 29.66288
	m_p (gr) 442.8189	g_p (mm) 200	h_4 (mm) 29.68952			

(a)

(b)
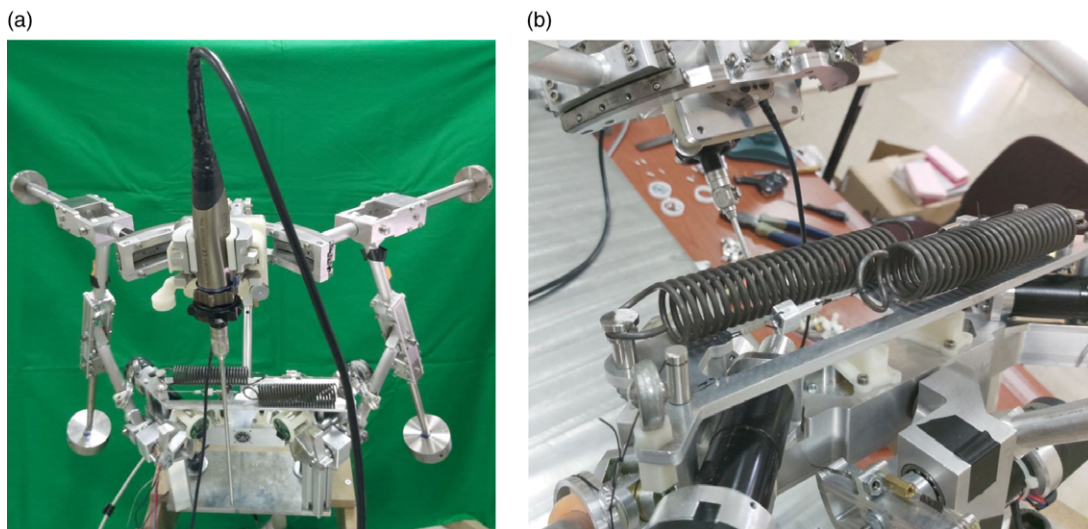
Figure 10. *(a) The assembled balanced prototype and (b) the springs and the tension adjustment component.*
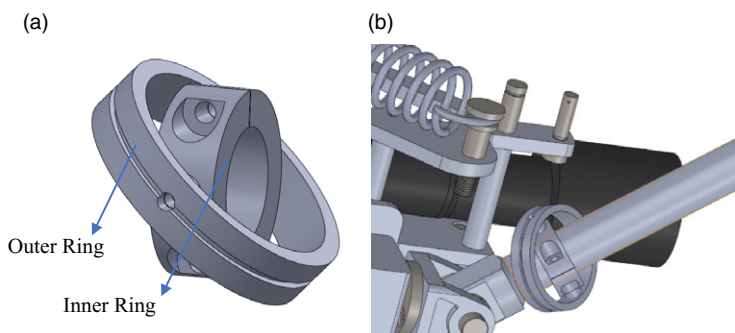
(a)

(b)

Outer Ring

Inner Ring

Figure 11. *(a) The connection part of the wire to the link and (b) the part assembled on the link.*

entry of the nostril. The torque values start to slightly increase when the tip of the endoscope reaches the surgery area where $d = 150$ mm.

$e = |A_0 C_a|$ and $f = |A_0 D_0|$ values (see Fig. 5) are determined according the constructional design. After the springs are manufactured and the spring coefficients are modified accordingly, e and f values are recalculated as seen in Table I.

4. Evaluation of the implemented static balancing methodology

After the calculations, the counter-mass components, the springs, and necessary connection compo- nents are manufactured. The manufactured spring coefficients are not exactly equal to the desired values. Simple tests with calibrated masses are performed to determine the spring coefficients of the manufac- tured springs. The coefficients are determined as $k_L = 1.804$ N/mm and $k_R = 1.592$ N/mm for the left and right leg balancing springs, respectively.

All manufactured balancing components are assembled on the prototype (Fig. 10). The two balancing springs are located on a plate fixed to the base platform of the manipulator. The wires are guided via

Table II. *Unbalanced – Balanced RMS torque comparison.*

Position #	Unbalanced RMS Torque (N·m)	Balanced RMS Torque (N·m)	% of Decline
1	4.67	0.91	95.96
2	2.53	0.35	86.17
3	2.57	1.81	29.35
4	2.55	1.49	41.57
5	1.91	2.95	−54.13
6	1.98	2.02	−1.98
7	1.08	1.93	−79.66
AVG RMS	2.47	1.53	37.84

an extra pin and spherical ball bearings between the spring and the proximal link. A tension adjustment component is manufactured to change the wire length for calibrating the springs.

The wires are connected to the links via two degree-of-freedom connection rings (Fig. 11). The inner ring is rigidly attached to the link, whereas the outer ring can rotate with respect to the inner ring and the wire within the grooves of the outer ring can rotate about the axis of the outer ring. It is observed that the endoscope can be manually repositioned quite easily.

Next, individual link balancing tests are performed by hanging the links with the counter-masses at their joint axes. Balancing condition is observed using water gauges and the locations of the cylinder blocks are slightly modified whenever necessary to achieve balanced links.

First, balancing tests for the manipulator are performed when the actuators are disabled in order to calibrate the springs (wire length and connection locations). It is observed that the endoscope can be manually located to any position within its workspace and static balance is obtained. These tests are important not to cause injuries to the patient in case of a motor failure. At every position, the end-effector location is measured using Faro Prime Arm – a coordinate measurement device. The targeted positions and the actual positions are in Table A.1 in Appendix A. It can be observed that the balanced manipulator can move to its boundary regions in each axis.

Finally, tests with functional actuators are performed with and without balancing components to see the effect of balancing on the actuator torques. During the measurements, it has been observed that the manipulator has some joint clearances. To measure the torque data of the motors, motor current values are monitored and also encoder data are recorded.

The balanced manipulator has been driven to the targeted positions via the motors, and once the endoscope is in the desired position, torque data have been collected. At each position of the manipulator, the endoscope position is measured with Faro Prime Arm. The torque and position data for the balanced manipulator are shown in Table A.2 in Appendix A.

From Table A.2, it can be seen that the position data from the encoder and Faro Prime Arm are different due to joint clearances in the mechanism. The position data from Faro Prime Arm have been accepted as the true position of the endoscope. In Table A.2, to see the general torque requirement at each position, the RMS torque values are calculated and also to see the general behavior average RMS torque has been calculated and the highest torque values for each leg and RMS torque are colored. Next, the balancing components are dismantled and tests are repeated for the unbalanced case. The resulting position and torque data are shown in Table A.3 in Appendix A.

When the manipulator's balancing components are removed, it is observed that the effect of joint clearances is increased which especially affected the heave motion. Again, at each position, RMS torque values are calculated, and also, the average RMS torque value is calculated and tabulated in Table A.3 with the maximum torque requirements colored in red. The RMS torque data for the balanced and unbalanced case are compared to see the effect of the balancing components (Table II). Lower torque values are recorded in most of the case for the balanced case. It should be pointed out that the end-effector could not be located at the same pose at all positions (please compare Tables A.2 and A.3). Nevertheless, the comparison concludes that the overall average torque requirement is about 37.8% less in the balanced

case. This is of course much less than 93.5% decrease, which was the result of simulations. The main reasons for the difference are the friction (which is not modeled in the simulations) and the joint clearances which result in joint flexibility.

5. Conclusions

In this study, a 2URRR-URR parallel manipulator is statically balanced using a hybrid spring and counter-mass balancing solution. Theoretically, each of the three legs can be balanced, but to avoid collisions with the passive serial arm, the payload mass is distributed to the legs on the sides. By adding counter-masses, distributed payload mass, distal and middle link masses are relocated to the proximal link, and the static balancing problem is reduced to balancing an inverted pendulum, which is achieved via a balancing spring.

With the additional balancing parts, the system's total mass is 10 kg which is within the allowable limits with respect to the design constraints. With balancing, the RMS torque of the motors is decreased from 3.08 N·m to 0.20 N·m which corresponds to a 93.5% decrease according to the simulation results.

Test results with the balanced manipulator without motors coupled to the mechanism indicate that the manipulator's end-effector can be statically balanced within its task space.

To measure the torque effects on the motors in the desired positions, the endoscope is positioned at several poses via the motors. The pose of the endoscope is measured with Faro Prime Arm. The differences between the desired and actual position data are the results of the joint clearances in the mechanism. The balancing components are removed from the manipulator and position, and torque data are recorded for the same set of positions of the endoscope. Based on these measurements, it is calculated that the average torque requirement from the motors is reduced by about 37.8% with balancing.

At the tested positions of the end-effector, the maximum torque requirement for the unbalanced case is 5.6 N·m (Table A.3), whereas it is 3.5 N·m for the balanced case (Table A.2). This is a significant decrease in terms of torque requirement and enhances the resolution of the actuators via enabling the choice of smaller actuators with less torque capacity.

The hybrid balancing methodology described in this work can be used for gravity balancing of parallel manipulators with articulated legs. Using counter-masses and springs for balancing have their respective advantages and disadvantages. With the proposed hybrid balancing solution, additional links are not used for the distal links, and the amount of additional mass is considerably reduced with the use of the spring for the proximal links.

References

[1] A. Martini, M. Troncossi, M. Carricato and A. Rivola, "Static balancing of a parallel kinematics machine with linear-delta architecture: Theory, design and numerical investigation," *Mech. Mach. Theory*, **90**, 128–141 (2015).

[2] M. Jean and C. M. Gosselin, "Static Balancing of Planar Parallel Manipulators," **In:** *Proceedings of IEEE International Conference on Robotics and Automation*, Minneapolis, Minnesota (1996) pp. 3732–3737.

[3] A. Russo, R. Sinatra and F. Xi, "Static balancing of parallel robots," *Mech. Mach. Theory*, **40**, 191–202 (2005).

[4] J. L. Herder, "Energy–Free Systems: Theory, Conception, and Design of Statically Balanced Spring Mechanisms," PhD thesis, Delft University of Technology (2001).

[5] A. Martini, M. Troncossi and A. Rivola, "Algorithm for the static balancing of serial and parallel mechanisms combining counter-weights and springs: generation, assessment and ranking of effective design variants," *Mech. Mach. Theory*, **137**, 336–354 (2019).

[6] J. Wang and X. Kong, "A geometric approach to the static balancing of mechanisms constructed using spherical kinematic chain units," *Mech. Mach. Theory*, **140**, 305–320 (2019).

[7] W. D. Van Dorsser, R. Barents, B. M. Wisse, M. Schenk and J. L. Herder, "Energy-free adjustment of gravity equilibrators by adjusting the spring stiffness," *IMechE C J. Mech. Eng. Sci.*, **222**(9), 1839–1846 (2008).

[8] A. Yaşir, G. Kiper, M. İ. C. Dede and V. Van der Wijk, "Static Force Balancing of a 2R1T Parallel Manipulator with Remote Center of Motion," **In:** *IFToMM WC 2019: Advances in Mechanism and Machine Science* (T. Uhl, ed.) (Springer, Cham, 2019) pp. 3219–3226.

[9] O. Maaroof, S. Z. Saeed and M. İ. C. Dede, "Partial gravity compensation of surgical robot," *Int. J. Adv. Robot. Syst.* **18**(3), 1–15 (2021).

[10] A. Yaşir, G. Kiper and M. İ. C. Dede, "Kinematic design of a non-parasitic 2R1T parallel mechanism with remote center of motion to be used in minimally invasive surgery applications," *Mech. Mach. Theory*, **153**, 104013 (2020).

[11] M. İ. C. Dede, G. Kiper, T. Ayav, B. Özdemirel, E. Tatlicioğlu, S. Hanalioglu, İ. Işikay and M. Berker, "Human–robot interfaces of the NeuRoboScope: A minimally invasive endoscopic pituitary tumor surgery robotic assistance system," *J. Med. Dev.* **15**(1), 011106 (2021).

[12] M. İ. C. Dede, G. Kiper, T. Ayav, G. Ateş, E. Tatlicioğlu, B. Özdemirel, O. Maaroof, M. Berker, İ. Işikay and ş. Hanalioğlu, "Cerrahın Anlık Yönlendirilebildiği Robot Yardımlı Endoskop Kontrol Sistemi Mimarisi – NeuRoboScope," **In:** *Türkiye Robotbilim Konferansı (TORK 2018)*, İstanbul (2018) pp. 25–30.

[13] O. W. N. Maaroof, "Design of a Robot Assisted Minimally Invasive Surgical System for Pituitary Tumor Surgery Based on Safety Features." PhD thesis, Izmir Institute of Technology (2020).

Appendix A

Table A.1. *Position data for balanced manipulator with disabled motors.*

	Targeted positions			Manually positioned		
Position #	d (mm)	ϕ (°)	ψ (°)	d (mm)	ϕ (°)	ψ (°)
1	250	0	0	250	1.623	7.588
2	200	0	0	200	0.642	1.52
3	150	0	0	150	1.213	0.785
4	150	−15	0	150	−17.425	−167
5	150	15	0	150	14.796	0.604
6	150	0	−20	150	3.975	−17.766
7	150	0	20	150	4.634	16.086

Table A.2. *Balanced manipulator position and torque data.*

	Balanced manipulator – Active motors									
	Encoder			FARO			Torque Results			
Position #	d (mm)	ϕ (°)	ψ (°)	d (mm)	ϕ (°)	ψ (°)	T_1 (N·m)	T_2 (N·m)	T_3 (N·m)	RMS $T.$ (N·m)
1	252.9	0.07	0.11	238.15	1.006	0.299	0.32	0.07	0.04	0.19
2	200.55	0.124	0.04	213.1	4.232	1.912	0.03	0.57	0.21	0.35
3	150.65	−0.06	−0.05	159.15	2.606	1.311	0.01	0.12	3.14	1.81
4	150.64	−20.52	−0.022	154.31	−16.809	−0.621	1.9	1.14	1.33	1.49
5	151.2	20.37	0.056	161.56	13.973	0.863	3.32	2.67	2.81	2.95
6	150.4	0.06	−20.643	125.63	0.692	−18.813	0.04	0.02	3.5	2.02
7	151.34	0.147	20.651	172.23	2.299	24.215	2.39	0.69	2.24	1.93
									AVG RMS	1.53

Table A.3. *Unbalanced manipulator with active motors position and torque values.*

	Unbalanced manipulator – Active motors									
	Encoder			FARO			Torque results			
Position #	d (mm)	$(\phi$ (°)	ψ (°)	d (mm)	ϕ (°)	ψ (°)	T_1 (N·m)	T_2 (N·m)	T_3 (N·m)	RMS $T.$ (N·m)
1	250.6	0.011	−0.37	230.33	0.919	−1.937	5.59	4.38	3.88	4.67
2	200	−0.02	−0.28	179.44	−1.216	−2.63	2.75	3.17	1.25	2.53
3	148.1	−0.01	−0.3	131.55	−0.78	−2.642	3.55	2.27	1.44	2.57
4	148.5	−15.44	−0.235	127.83	−13.422	−1.33	2.69	1.3	2.04	2.55
5	148.9	15.465	−0.18	134.94	15.762	−1.286	1.86	1.41	2.35	1.91
6	149.65	−0.04	−20.76	123.04	−0.916	−19.675	1.04	1.42	2.95	1.98
7	150.3	−0.04	20.46	155.51	−1.215	20.23	1.22	1.41	0.07	1.08
									AVG RMS	2.47